Chinese Chemical Letters 35 (2024) 109759

Contents lists available at ScienceDirect

Chinese Chemical Letters

journal homepage: www.elsevier.com/locate/cclet

Penicillin G acylase-responsive near-infrared fluorescent probe: Unravelling biofilm regulation and combating bacterial infections

Yang Liu, Leilei Zhang*, Kaixuan Liu, Ling-Ling Wu*, Hai-Yu Hu*

State Key Laboratory of Bioactive Substance and Function of Natural Medicines, Beijing Key Laboratory of Active Substance Discovery and Druggability Evaluation, Institute of Materia Medica, Chinese Academy of Medical Sciences & Peking Union Medical College, Beijing 100050, China

ARTICLE INFO

Article history:
Received 6 February 2024
Revised 6 March 2024
Accepted 8 March 2024
Available online 9 March 2024

Keywords:
Penicillin G acylase
Phototherapy
Biofilm regulation
Wound healing
Photothermal
Photodynamic

ABSTRACT

Antibiotic resistance poses a critical threat to human healthcare, largely driven by bacterial biofilms. These biofilms resist the immune system and antibiotics, rendering enclosed microbial cells 10–1000 times more antibiotic-resistant than planktonic cells, leading to severe infections. Therefore, there is an urgent need to develop innovative tools for investigating biofilm regulators and devising novel antibacterial strategies. In this study, we developed **Cy-NEO-PA**, a near-infrared (NIR) fluorescent probe responsive to penicillin G acylase (PGA), with bacteria-targeting ability. This probe was designed to visualize the influence of environmental factors on biofilm formation in *Acinetobacter baumannii* (*A. baumannii*). Our findings demonstrated that glucose suppressed PGA production, leading to enhanced biofilm formation, whereas phenylacetic acid (PAA) stimulated PGA production and inhibited biofilm formation in *A. baumannii*. These observations highlight the remarkable capability of **Cy-NEO-PA** to accurately measure PGA dynamics, shedding light on the critical role of PGA in biofilm development. Additionally, **Cy-NEO-PA** exhibited excellent biocompatibility, potent reactive oxygen species (ROS) generation, efficient photothermal conversion, and bacteria-targeting abilities, making it a promising agent for combating bacterial infections and promoting wound healing through photothermal (PTT)/photodynamic (PDT) therapy. These discoveries emphasize the significant role of PGA in antibacterial therapy and offer valuable insights for the design of effective strategies targeting PGA to combat biofilm-associated infections.

Acinetobacter baumannii (*A. baumannii*), a critical Gram-negative strain among the ESKAPE pathogens (*Enterococcus faecium*, *Staphylococcus aureus*, *Klebsiella pneumoniae*, *Acinetobacter baumannii*, *Pseudomonas aeruginosa*, and *Enterobacter* species), presents a significant public health threat due to its robust biofilm-forming capabilities, which enhance persistence and virulence [1–3]. The extracellular polymeric substance matrix within the biofilm acts as a protective barrier, impeding antibiotic penetration and resulting in heightened resistance [4–6]. Although antibiotics are the primary treatment, the emergence of multidrug-resistant (MDR) strains necessitates the exploration of alternative approaches. Therefore, understanding the regulatory mechanisms of *A. baumannii* biofilm formation and developing innovative therapeutic strategies are crucial to achieving successful treatment outcomes. Antibacterial phototherapy (APT), especially the combination of photodynamic (PDT) and photothermal (PTT) therapy, has emerged as a promising approach due to its precise spatiotemporal control, non-invasiveness, low resistance, and minimal systemic toxicity [7–15]. However, the development of phototherapeutic agents (PTAs) with bacterial biotarget specificity remains a scientific challenge. Ideally, PTAs should self-regulate reactive oxygen species (ROS) production and photothermal conversion, exhibiting low activity in normal tissue but strong activation at the site of bacterial infection, enabling selective and efficient phototherapy. Such advancements would enable the development of highly selective and efficient phototherapy techniques to combat bacterial infections, effectively targeting drug-resistant bacteria and disrupting the formation of biofilms.

Penicillin G acylase (PGA, EC 3.5.1.11) has been widely utilized in pharmaceutical production for over 50 years, enabling eco-friendly synthesis of key intermediates for β-lactam antibiotics [16–19]. Recently, PGA has also been studied for its applications in the site-selective functionalization of insulin [20]. Despite the well-established knowledge of its enzyme structure, physicochemical characterization, and industrial applications, the physiological roles of PGA in bacterial signaling and pathogenesis have often been overlooked [21]. Recent investigations have revealed the efficient hydrolytic activity of acylase enzymes derived from Gram-negative bacteria on *N*-acyl-homoserine lactones (AHLs), the quorum

* Corresponding authors.
E-mail addresses: zhangleilei@imm.ac.cn (L. Zhang), wll1950797436@hotmail.com (L.-L. Wu), haiyu.hu@imm.ac.cn (H.-Y. Hu).

https://doi.org/10.1016/j.cclet.2024.109759
1001-8417/

sensing signal molecules, resulting in reduced virulence during biofilm formation [22,23]. In *A. baumannii*, AHL signaling molecules play a crucial role in cell-to-cell communications, which significantly impacts its biofilm formation [24–27]. As a result, it is hypothesized that PGA may have a significant role in this process. However, the specific contribution of PGA to *A. baumannii* biofilm formation remains unclear and further research in this area would provide valuable insights.

Although several small molecule fluorescent probes have been reported for detecting PGA activity and screening natural inhibitors, few of them are suitable for bacteria imaging and antibacterial treatment [28–33]. In this study, we developed a novel bacteria-targeting near-infrared (NIR) fluorescent probe, **Cy-NEO-PA**, for real-time detection of PGA activity in *A. baumannii* (Scheme 1). The probe allowed visualization of how environmental factors influence PGA activity and impact biofilm formation in MDR *A. baumannii*. Glucose was found to suppress PGA production, leading to enhanced biofilm formation, while phenylacetic acid (PAA) stimulated PGA production and inhibited biofilm formation. These insights highlight the intricate relationship between PGA activity, environmental cues, and biofilm formation.

Additionally, **Cy-NEO-PA** exhibited targeted activation at the site of bacterial infection, leading to potent ROS generation and efficient photothermal conversion, making it a promising agent for combating bacterial infections and promoting wound healing through photothermal/photodynamic therapy. The PGA-responsive probe holds significant potential as a highly promising therapeutic approach for addressing bacterial infections.

PGA has demonstrated promising potential in AHLs degradations, leading to the attenuation of virulence associated with Gram-negative bacterial biofilm formations [34,35]. In order to visualize and gain insights into how various environmental factors influence PGA activity and its subsequent impact on biofilm formation in MDR *A. baumannii*, we developed a novel PGA-responsive NIR probe, **Cy-NEO-PA**, based on PGA's hydrolase properties (Scheme 1). Recently, we successfully devised an efficient molecular design strategy for constructing analyte-activated PA probes utilizing heptamethine cyanine (Cy7) fluorophore [36]. By substituting Cy7 with *p*-aminophenyl (**Cy-NEO-NH$_2$**), we achieved a remarkable enhancement in non-radiative relaxation and photothermal efficacy. The selective incorporation of a phenylacetyl group, recognized and hydrolyzed by PGA, effectively inhibited the excited-state photoinduced electron transfer (a-PeT) process, leading to fluorescence recovery. Furthermore, we strategically integrated neomycin, a Gram-negative bacterial lipopolysaccharide-targeting moiety, into the probe to enhance water solubility and facilitate precise bacterial targeting [37–39]. **Cy-NEO-PA** exhibited robust initial fluorescence, which was subsequently quenched upon PGA interaction, resulting in the formation of **Cy-NEO–NH$_2$** (Fig. S3 in Supporting information). Comprehensive synthetic routes and characterization data for **Cy-NEO-PA** and its product **Cy-NEO–NH$_2$** were provided in the supporting information.

We conducted a comprehensive investigation into the photophysical properties of both **Cy-NEO-PA** and its product, **Cy-NEO–NH$_2$**. Both probes exhibited similar absorption spectra with a maximum peak observed at 770 nm (Fig. 1A). However, a significant difference was observed in their fluorescence spectra. **Cy-NEO-PA** displayed a robust fluorescence emission peak at 787 nm, whereas **Cy-NEO–NH$_2$** showed negligible fluorescence emission (Fig. 1B). Furthermore, we determined the molar absorption coefficient and fluorescence quantum yield (Fig. S2 in Supporting information), revealing a remarkable 40-fold higher fluorescence quantum yield for **Cy-NEO-PA** ($\Phi_f = 23.96\%$) compared to **Cy-NEO–NH$_2$** ($\Phi_f = 0.61\%$), with minimal variation in the molar absorption coefficient.

The response of the probe **Cy-NEO-PA** to PGA was investigated by analyzing its optical properties in the presence or absence of PGA. Optimal fluorescence signal difference was observed under physiological conditions, at approximately pH 7.4 and a temperature of 37 °C (Fig. S4 in Supporting information). Fluorescence spectra were measured across various concentrations of PGA (Fig. 1C), revealing gradually notable differences in fluorescence intensity with increasing PGA concentrations. The relationship displayed linearity within the range of 0 to 0.8 U/mL (Fig. 1D), with a detection limit of 0.041 U/mL. Calculated values for the Michaelis constant (K_m) and maximum reaction rate (V_{max}) of the **Cy-NEO-PA** probe towards PGA were 4.24 μmol/L and 0.0066 μmol L^{-1} s^{-1}, respectively (Fig. S5 in Supporting information). The specificity of **Cy-NEO-PA** towards PGA was confirmed, as various biological analytes did not cause significant changes in fluorescence intensity (Fig. 1E). Additionally, the near-infrared fluorescent (NIRF) signals were recovered, when the PGA inhibitor (100 mmol/L penicillin) was added, further confirming the probe's high selectivity towards PGA (Fig. 1F).

The biocompatibility of the probe is crucial for its imaging application in living cells. Hence, we evaluated the cytotoxicity of both **Cy-NEO-PA** and **Cy-NEO–NH$_2$** on HepG2, U343, and BIU-87 cell lines using the cell counting kit-8 (CCK-8) assay. At the concentration of 10 μmol/L, which is used for live cell imaging, both the probe and its product had minimal impact on cell viability, indicating low cytotoxicity and good biocompatibility (Fig. S6 in Supporting information). Next, we explored the potential of the **Cy-NEO-PA** probe for real-time sensing of endogenous PGA activity in living bacterial cells using confocal laser scanning microscopy (CLSM). As depicted in Fig. 2, minimal fluorescence was observed in *A. baumannii* (ATCC 19606) and MDR *A. baumannii* (Bio-53272) when the probe was applied. However, fluorescence recovery was observed when the probe was applied to the bacteria in the presence of a PGA inhibitor, penicillin (100 mmol/L). CLSM investiga-

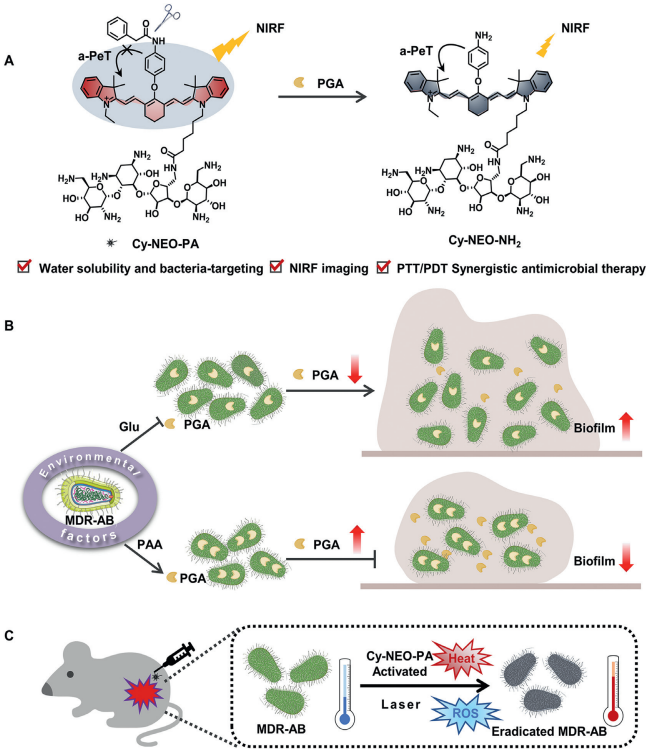

Scheme 1. Schematic diagram of the application of PGA responsive probe: (A) Illustration of PGA-responsive fluorescent probe, **Cy-NEO-PA**. (B) The influence of environmental factors on PGA activity and biofilm formation. (C) Synergistic PTT/PDT therapy under NIR light irradiations.

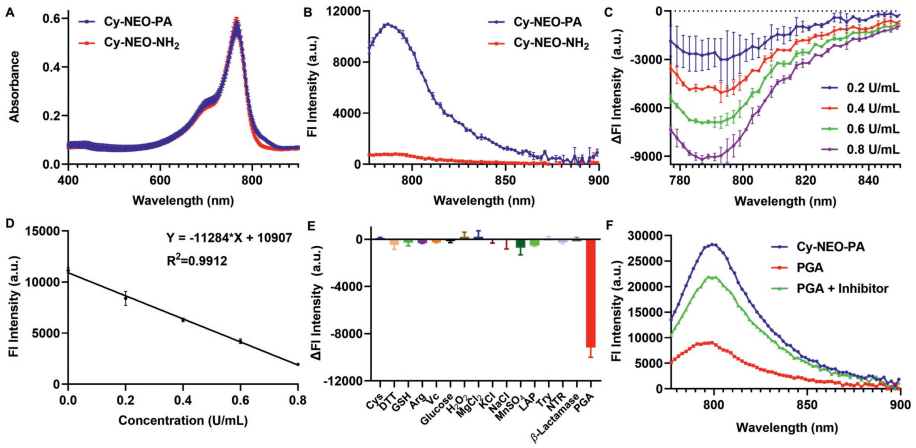

Fig. 1. Optical spectra and the response of **Cy-NEO-PA** to PGA. (A) UV–vis–NIR absorption spectra and (B) fluorescence emission spectra of **Cy-NEO-PA** and **Cy-NEO-NH$_2$** (10 μmol/L) in Tris buffer containing 1.5% DMSO. (C) Relative fluorescence response of **Cy-NEO-PA** to different amounts of PGA (0.2 U/mL, 0.4 U/mL, 0.6 U/mL, and 0.8 U/mL) in Tris buffer at 37 °C. (D) The linear relationship between the PGA concentration and fluorescence intensity (λ_{ex} = 740 nm, λ_{em} = 785 nm). (E) Relative fluorescence response of **Cy-NEO-PA** upon the addition of PGA (1 U/mL) and other biologically important factors, cysteine (Cys, 1 mmol/L), dithiothreitol (DTT, 1 mmol/L), glutathione (GSH, 1 mmol/L), arginine (Arg, 1 mmol/L), vitamin C (Vc, 1 mmol/L), glucose (10 mmol/L), H_2O_2 (10 mmol/L), $MgCl_2$ (2.5 mmol/L), KCl (10 mmol/L), NaCl (10 mmol/L), $MnSO_4$ (10 mmol/L), leucine aminopeptidase (LAP, 0.06 U/mL), trypsin (Try, 25 μg/mL), NTR (1 μg/mL nitroreductase, 500 μmol/L NADH), β-lactamase (1 U/mL) (λ_{ex} = 740 nm, λ_{em} = 785 nm). (F) Fluorescence intensity for **Cy-NEO-PA** (10 μmol/L) upon reaction with PGA (1 U/mL) in Tris-buffer saline with or without PGA inhibitor, penicillin (100 mmol/L) using 1.5% DMSO and 0.1% Kolliphor RH40 as co-solvent (pH 7.4), at 37 °C (λ_{ex} = 740 nm, λ_{em} = 785 nm). Error bar: mean ± standard deviation (SD) (n = 3).

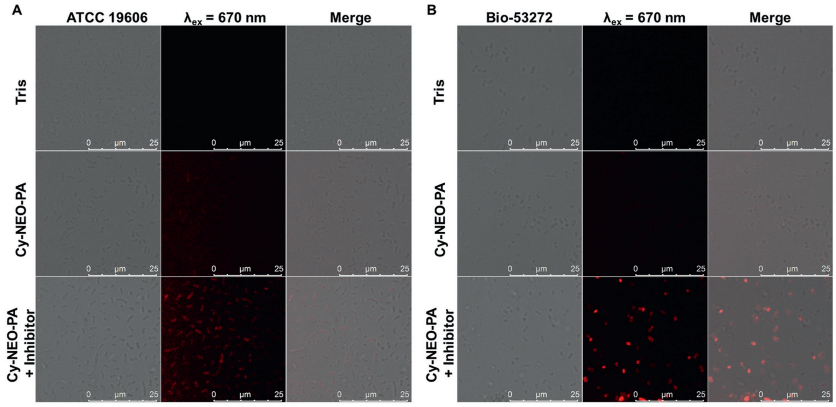

Fig. 2. Confocal fluorescence images of (A) live *A. baumannii* (ATCC 19606, OD_{600} = 0.5) and (B) MDR *A. baumannii* (Bio-53272, OD_{600} = 0.5) visualized with **Cy-NEO-PA** (10 μmol/L) with or without PGA inhibitor, penicillin (100 mmol/L) in Tris buffer (pH 7.4, containing 1.5% DMSO and 0.1% Kolliphor RH40 as co-solvent).

tions indicated that **Cy-NEO-PA** was readily taken up by bacterial cells and interacted with PGA, resulting in the generation of the enzyme reaction product **Cy-NEO–NH$_2$** and subsequent fluorescence quenching. In order to directly observe the targeted recognition of probe molecules to bacteria, we explored the selective labeling potential of **Cy-NEO-PA** by CLSM imaging of *A. baumannii* after co-culture with mammalian Raw 264.7 cells (Fig. S7 in Supporting information). The results demonstrated that **Cy-NEO-PA** could accurately visualize *A. baumannii* in the co-culture system with mammalian host cells. Moreover, these findings were proved by enzyme-linked immunosorbent assay (ELISA) results (Fig. S8 in Supporting information) and underscore the potential of **Cy-NEO-PA** as an effective "turn-off" fluorescent sensor for PGA activity in *A. baumannii*.

The biofilm formation process in Gram-negative bacteria is influenced by a variety of biological and environmental factors, including KCl, $MgCl_2$, $CaCl_2$, glucose, galactose, glycine, glycerol, and PAA [40–42]. To investigate the impact of these factors on PGA activity and biofilm formation in *A. baumannii*, we utilized the probe **Cy-NEO-PA**. Fig. 3A showed that glucose (Glu) and PAA have a significant impact on PGA activity. Further investigations (Figs. 3B and C) revealed that PAA played a crucial role as a potent promoter, leading to a significant increase in PGA production when its concentration exceeded 0.03% (equivalent to 0.3 g/L). At a concentration of 0.05%, PAA induced a remarkable 140% increase in PGA activity after overnight incubation. In contrast, glucose exhibited an inhibitory effect on PGA activity, with concentrations ranging from 0.5% to 1%. Additionally, the biomass of *A. baumannii* biofilm was evaluated using the crystal violet staining assay [43]. These results demonstrated that the addition of 0.5% and 1% glucose significantly enhanced biofilm formation in a concentration-dependent manner compared to the control without glucose. Conversely, the presence of PAA at concentrations of 0.03% and 0.05% suppressed biofilm growth, resulting in a 20% reduction in biofilm mass at a concentration of 0.05% compared to the control (Figs. 3D–F). These findings strongly suggest a negative correlation between PGA expression and the biofilm formation process of *A. baumannii*. It is likely that PGA's ability to degrade AHLs plays a role in attenuating virulence through quorum quenching. These significant findings may pave the way for the development of novel antibacterial strategies.

Phototherapy is a promising treatment method widely used in clinics for its localized application, minimal invasiveness, cost-effectiveness, broad antimicrobial activity, and low side effects [44–46]. The probe **Cy-NEO-PA** and the product **Cy-NEO-NH$_2$** show potential for both photodynamic and photothermal synergistic therapy as they can convert light energy into heat and, at the

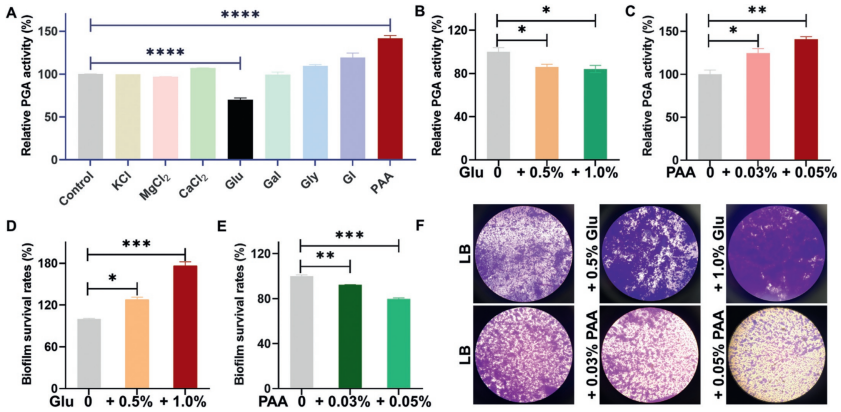

Fig. 3. Relative changes of PGA activity and biofilm formation in response to different environmental factors. (A) Effects of environmental factors on PGA activity and biofilm formation. The relative PGA activity in the presence of different amounts of (B) glucose and (C) PAA. The survival rate of the biofilm was determined by crystal violet staining in the presence of (D) glucose and (E) PAA. (F) Optical microscope photographs of residual biofilms after treatment with different incubation conditions, stained by crystal violet. $^{*}P < 0.05$, $^{**}P < 0.01$, $^{***}P < 0.001$, $^{****}P < 0.0001$. Error bar: mean ± SD ($n = 3$).

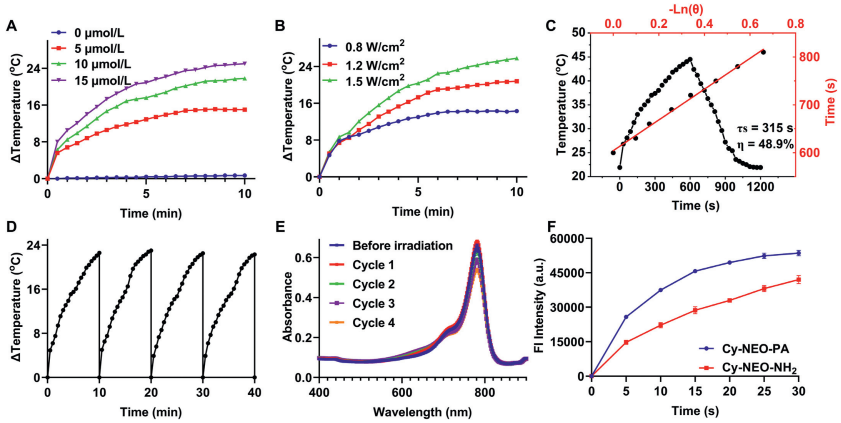

Fig. 4. Photothermal and photodynamic properties of **Cy-NEO-PA** and **Cy-NEO-NH$_2$**. (A) Photothermal heating curves of **Cy-NEO-NH$_2$** at different concentrations under NIR irradiation (785 nm laser, 1.2 W/cm^2). (B) The temperature increases of **Cy-NEO-NH$_2$** under various intensities of NIR irradiation. (C) Photothermal effect of **Cy-NEO-NH$_2$** under laser irradiation for heating and cooling period (1.2 W/cm^2). (D) The temperature changes of **Cy-NEO-NH$_2$** during four cycles of heating-cooling processes under irradiation at 1.2 W/cm^2. (E) UV–vis absorbance spectra of **Cy-NEO-NH$_2$** over four cycles of irradiation. (F) The fluorescence intensity of DCFH reacted with ROS generated by **Cy-NEO-PA** and **Cy-NEO-NH$_2$** under laser irradiation (785 nm, 1.2 W/cm^2).

same time, produce ROS when exposed to light. The photothermal characteristics of **Cy-NEO-PA** and **Cy-NEO-NH$_2$** were systematically evaluated. As depicted in Fig. 4 and Fig. S10 (Supporting information), **Cy-NEO-NH$_2$** demonstrated a higher temperature elevation under NIR irradiation compared to **Cy-NEO-PA**. Notably, increasing the concentration of the two compounds resulted in a corresponding elevation in temperature under identical irradiation conditions. Moreover, as the power density increased, the temperature of both compounds exhibited a gradual rise. After careful optimization, a medium probe concentration (10 μmol/L) and laser power (785 nm, 1.2 W/cm^2) were selected, resulting in a rapid 22 °C temperature increase in the **Cy-NEO-NH$_2$** solution. Further analysis of the heating-cooling curves, incorporating the associated time constant (τs), enabled the determination of the photothermal conversion efficiency (η) of **Cy-NEO-NH$_2$**, which was found to be 48.9% [47]. To assess the photothermal stability of **Cy-NEO-NH$_2$**, heating-cooling curves were generated over four cycles of irradiation. Remarkably, these curves revealed minimal temperature and UV absorbance decline, indicating a high resistance to photobleaching for **Cy-NEO–NH$_2$**. Then, the PDT study was carried out to assess ROS production induced by NIR light using the dichlorodihydrofluorescein diacetate (DCFH-DA) assay [48]. Both **Cy-NEO-PA** and **Cy-NEO–NH$_2$** exhibited significant elevation in ROS levels upon NIR irradiation (785 nm, 1.2 W/cm^2) for 30 s. These findings confirmed the excellent photothermal performance and photodynamic capabilities of **Cy-NEO-PA** and **Cy-NEO–NH$_2$**, making it a promising dual-mode agent for combined PTT and PDT therapy.

Subsequently, the *in vitro* antibacterial activity of **Cy-NEO-PA** was assessed using both a plate counting assay and the calcein-AM/propidium iodide (PI) dual fluorescence death-and-live staining method [49]. The MIC values of **Cy-NEO-PA** and **Cy-NEO–NH$_2$** for *A. baumannii* strains, including ATCC 19606 and MDR Bio-53272 strains, were determined. Without light irradiation, both compounds exhibited negligible toxicity at 50 μmol/L (Table S1 in Supporting information). However, as shown in Figs. S11 and S12 (Supporting information), **Cy-NEO-PA**-mediated phototherapy (785 nm, 1.2 W/cm^2) demonstrated a significant ability to disrupt both *A. baumannii* and MDR *A. baumannii*. The employed staining methodology involved using Calcein-AM for green fluorescent staining of live bacteria, while PI could selectively penetrate damaged membranes, resulting in red staining of dead bacteria. Fig. S12 illustrates that the Laser group predominantly exhibited green fluorescence, whereas the **Cy-NEO-PA** + Laser groups for both *A. baumannii* and the MDR strain displayed primarily red fluorescence. This observation suggests substantial bacterial cell death following **Cy-NEO-PA**-mediated phototherapy. To elucidate the inhibitory mechanism of the probe, we employed scanning electron microscopy (SEM), which unveiled pronounced morphological alterations and disrup-

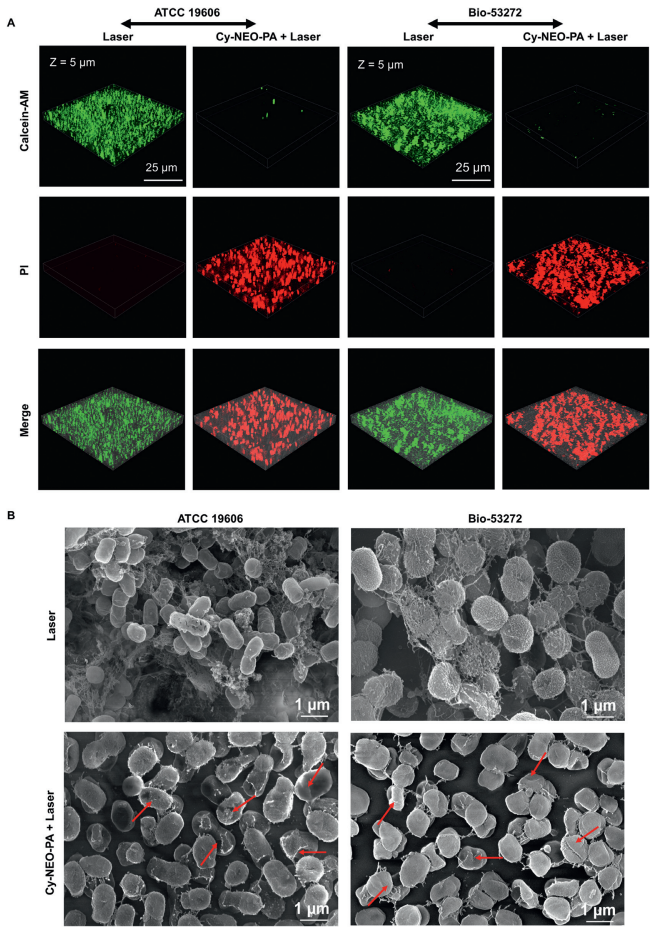

Fig. 5. Antibiofilm activity study of **Cy-NEO-PA** under laser irradiation. (A) Calcein-AM/PI dual staining fluorescence images of *A. baumannii* biofilm (green color, living bacteria; red color, dead bacteria) without or with **Cy-NEO-PA** (10 μmol/L) under laser irradiation (785 nm, 1.2 W/cm^2). (B) SEM images of *A. baumannii* biofilm under light irradiations without or with **Cy-NEO-PA** treatment.

tion of bacterial membranes in the **Cy-NEO-PA** treated group. In the Laser group (without the probe), bacterial exhibited the characteristic smooth and intact surfaces of both *A. baumannii* and the MDR strain. In contrast, the **Cy-NEO-PA**-mediated phototherapy group exhibited pronounced alterations in bacterial cell morphology, with cells becoming rougher and fragmented, and even experiencing severe collapse of the cell wall/membrane.

Notably, approximately 80% of persistent and recalcitrant chronic infections can be attributed to the presence of biofilms. Once a bacterial biofilm is established, it can adeptly evade the host immune system and concurrently exhibit increased resistance to antibiotic treatments. This presents a formidable challenge compared to planktonic bacteria. In this work, we further evaluated the antibiofilm potential of **Cy-NEO-PA**-mediated phototherapy. Crystal violet staining results demonstrated a dose-dependent reduction in biofilm formation in both *A. baumannii* (ATCC 19606) and its MDR strain (Bio-53272). Specially, pretreatment of *A. baumannii* with the probe under irradiation significantly suppressed biofilm formation, while *A. baumannii* exposed to light alone continued to form biofilms under the same conditions. At a probe concentration of 10 μmol/L, a noteworthy inhibition rate of up to 70% was observed (Fig. S13 in Supporting information). The results of calcein-AM/PI dual fluorescence staining shown in Fig. 5A verify that the **Cy-NEO-PA**-mediated phototherapy could effectively eliminate the bacterial biofilm. The biofilms of the laser groups all emitted bright green fluorescence which is indicative of live bacteria. On the contrary, the intense red fluorescence emitting from the **Cy-NEO-PA** + Laser groups definitely indicate the elimination of the bacteria as the result of the **Cy-NEO-PA** induced treatment. These results were in good agreement with Crystal violet staining results. Furthermore, scanning electron microscope studies corroborated a substantial reduction in biofilm formations upon **Cy-NEO-PA** treatment under irradiation (Fig. 5B). Typically, photothermal treatment leads to the destruction of the outermost layer of the bacterial cell wall, while the increased levels of ROS facilitate the penetration of the bacterial membrane, causing protein loss due to membrane disruption and ultimately resulting in bacterial death [50]. These observations strongly support the hypothesis that **Cy-NEO-PA**-induced photothermal/photodynamic synergistic therapy significantly enhances bacterial membrane permeation, ultimately leading to bacterial death and inhibition of biofilm formation.

Encouraged by the promising *in vitro* phototherapeutic properties of **Cy-NEO-PA**, we conducted *in vivo* evaluations to combat bacterial infections. All animal experiments were conducted in accordance with the guidelines of the Committee on Animals at the Institute of Materia Medica, Chinese Academy of Medical Sciences & Peking Union Medical College (Beijing, China) and were approved by the Ethical Committee (Approval number: 00005182). In the mouse model of MDR *A. baumannii* (Bio-53272) skin infection, time-dependent photothermal imaging was performed using handheld thermography. After injecting 50 μL of 20 μmol/L **Cy-NEO-PA** at the wound site, the wound was irradiated with a laser (785 nm, 1.2 W/cm^2) for 5 min at various time points: 0, 0.5, 1, 2, 4, and 6 h post-injection. Under near-infrared laser irradiation, **Cy-NEO-PA** exhibited excellent photothermal performance, with a temperature increase of approximately 15 °C within 0.5 h and reaching 45 °C, followed by a decline at later time points (Fig. S14 in Supporting information). Furthermore, the antibacterial activity of **Cy-NEO-PA** was evaluated by administering the probe *via in situ* injection at a concentration of 20 μmol/L in a volume of 50 μL for 4 days. The wounds were then exposed to laser irradiation (785 nm, 1.2 W/cm^2) for 5 min (Fig. 6A). Wound healing was monitored over time, and the **Cy-NEO-PA** + Laser group exhibited faster crust detachment and the most rapid wound closure rates. By day 12, the **Cy-NEO-PA** + Laser treated mice displayed a significantly reduced wound area and more apparent scars, with an average wound closure rate of approximately 80%, while the other groups took longer to heal (wound closure rate less than 40%) (Figs. 6B and C, Fig. S15 in Supporting information). This demonstrated that phototherapy mediated by **Cy-NEO-PA** significantly enhanced the healing of skin wounds by effectively combating bacterial infections. Importantly, no significant weight loss was observed during the course of phototherapy, indicating the treatment did not induce any apparent toxicity (Fig. 6D, Fig. S16 in Supporting information). For a better understanding of the wound healing process under different treatments, hematoxylin and eosin (H&E) staining was performed to evaluate the inflammation of the infected wound tissue (Fig. 6E). On day 12 post-phototherapy, the **Cy-NEO-PA** + Laser group showed minimal infiltration of inflammatory cells and a normal skin structure compared to the other groups, suggesting phototherapy promoted skin tissue repair. These observations were consistent with the wound healing results.

We have successfully developed a novel PGA-responsive near-infrared fluorescent probe, **Cy-NEO-PA**, with significantly enhanced fluorescence sensitivity, enabling precise visualization of PGA activity in *A. baumannii*. Using this probe, we investigated the impact of environmental factors on PGA activity and biofilm formation, revealing the regulatory roles of glucose and PAA in these processes. Notably, glucose and PAA also exert similar regulatory effects on PGA activity and biofilm formation in both *Pseudomonas aeruginosa* and *Escherichia coli* (Fig. S9 in Supporting information). Furthermore, **Cy-NEO-PA** demonstrated high efficiency in ROS production,

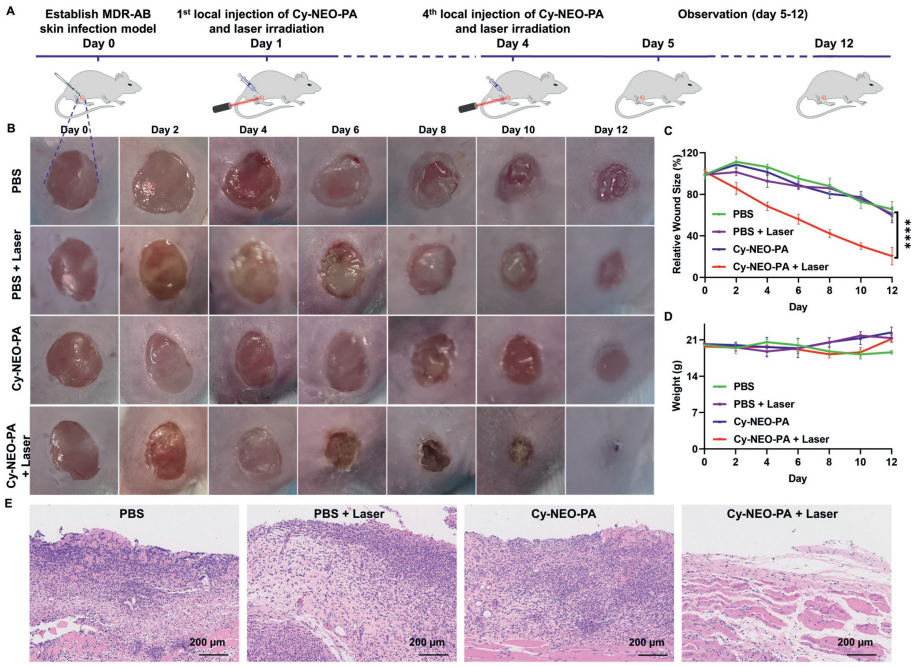

Fig. 6. NIR light-mediated photodynamic and photothermal synergistic therapeutics in mouse skin infection model. (A) The establishment of an *in vivo* MDR-AB skin infection model and the treatment procedures: medication and laser administration were performed once per day for the initial 4 days of the experiments. (B) Images of skin-infected wounds under different treatments. (C) The relative changes of wound area ($n = 6$). (D) Body weights of mice during different treatments. (E) Microscopic images of the infected tissue sections (H&E staining) in each group. $^{****}P < 0.0001$. Error bar: mean ± SD ($n = 6$).

photothermal conversion, and excellent biocompatibility, positioning it as a promising candidate for NIR-induced PTT/PDT synergistic therapy against bacterial infections and biofilm formations. This approach effectively enhances antibacterial efficacy by combining heat-induced bacterial damage with ROS cytotoxicity. The development of **Cy-NEO-PA** as a PGA-responsive near-infrared fluorescent probe provides valuable insights into environmental factors, PGA dynamics, and biofilm formations, holding great promise as a non-invasive, selective, and effective strategy for treating biofilm-associated infections.

Declaration of competing interest

The authors declare that they have no known competing financial interests or personal relationships that could have appeared to influence the work reported in this paper.

Acknowledgments

This work was supported by the National Natural Science Foundation of China (NSFC) projects (Nos. 22122705, 22077139), National Key R&D Program of China (No. 2022YFE0199700), CAMS Innovation Fund for Medical Sciences (CIFMS) (No. 2021-I2M-1-054), and the Disciplines Construction Project (No. 201920200805).

Supplementary materials

Supplementary material associated with this article can be found, in the online version, at doi:10.1016/j.cclet.2024.109759.

References

[1] A. Gedefie, W. Demsiss, M.A. Belete, et al., Infect. Drug Resist. 14 (2021) 3711–3719.
[2] C.R. Lee, J.H. Lee, M. Park, et al., Front. Cell. Infect. Microbiol. 7 (2017) 55.
[3] K.G. Dolma, R. Khati, A.K. Paul, et al., Biology 11 (2022) 1343.
[4] C. Uruén, G. Chopo-Escuin, J. Tommassen, R.C. Mainar-Jaime, J. Arenas, Antibiotics 10 (2021) 3.
[5] A. Singh, A. Amod, P. Pandey, et al., Biomed. Mater. 17 (2022) 022003.
[6] S.G. Mendes, S.I. Combo, T. Allain, et al., Eur. J. Clin. Microbiol. Infect. Dis. 42 (2023) 1405–1423.
[7] H. Zhang, C. He, L. Shen, et al., Chin. Chem. Lett. 34 (2023) 108160.
[8] Q. Zhao, G. Qing, J. Yu, et al., Chin. Chem. Lett. 35 (2023) 108535.
[9] G. Wei, G. Yang, Y. Wang, et al., Theranostics 10 (2020) 12241–12262.
[10] M. Ribeiro, I.B. Gomes, M.J. Saavedra, M. Simões, Lett. Appl. Microbiol. 75 (2022) 548–564.
[11] A. Mathur, A.S. Parihar, S. Modi, A. Kalra, Microb. Pathog. 183 (2023) 106307.
[12] A. Cruz, M. Condinho, B. Carvalho, et al., Antibiotics 10 (2021) 1482.
[13] A. Warrier, N. Mazumder, S. Prabhu, K. Satyamoorthy, T.S. Murali, Photodiagnosis Photodyn. Ther. 33 (2021) 102090.
[14] J. Huo, Q. Jia, H. Huang, et al., Chem. Soc. Rev. 50 (2021) 8762–8789.
[15] W. Xiu, L. Wan, K. Yang, et al., Nat. Commun. 13 (2022) 3875.
[16] A. Bruggink, E.C. Roos. Eric, E. Vroom, Org. Process Res. Dev. 2 (1998) 128–133.
[17] A.K. Chandel, L.V. Rao, M.L. Narasu, O.V. Singh, Enzyme Microb. Tech. 42 (2008) 199–207.
[18] H. Marešová, M. Plačková, M. Grulich, P. Kyslík, Appl. Microbiol. Biot. 98 (2014) 2867–2879.
[19] L. Li, L. Feng, M. Zhang, et al., Chem. Commun. 56 (2020) 4640–4643.
[20] A. Fryszkowska, C. An, O. Alvizo, G. Banerjee, et al., Science 376 (2022) 1321–1327.
[21] V.S. Avinash, A.V. Pundle, S. Ramasamy, C.G. Suresh, Crit. Rev. Biotechnol. 36 (2016) 303–316.
[22] A.V. Sunder, P.D. Utari, S. Ramasamy, et al., Appl. Microbiol. Biotechol. 101 (2017) 2383–2395.
[23] R. Velasco-Bucheli, D. Hormigo, J. Fernández-Lucas, et al., Catalysts 10 (2020) 730.
[24] L. Zhou, Y. Zhang, Y. Ge, X. Zhu, J. Pan, Front. Microbiol. 11 (2020) 589640.
[25] B. Cui, X. Chen, Q. Guo, et al., Microbiol. Spectr. 10 (2022) e0102722.
[26] K. Saipriya, C.H. Swathi, K.S. Ratnakar, V. Sritharan, J. Appl. Microbiol. 128 (2020) 15–27.
[27] N.G. Naga, D.E. El-Badan, K.M. Ghanem, M.I. Shaaban, Cell Commun. Signal. 21 (2023) 133.
[28] E. Danieli, D. Shabat, Bioorg. Med. Chem. 15 (2007) 7318–7324.
[29] J.A. Richard, M. Massonneau, P.Y. Renard, A. Romieu, Org. Lett. 10 (2008) 4175–4178.
[30] S. Debieu, A. Romieu, Org. Biomol. Chem. 15 (2017) 2575–2584.
[31] S. Jenni, F. Ponsot, P. Baroux, et al., Spectrochim. Acta. A: Mol. Biomol. Spectrosc. 248 (2021) 119179.
[32] S. Debieu, A. Romieu, Org. Biomol. Chem. 13 (2015) 10348–10361.
[33] C. Zhao, W. Sun, B. Tan, D. Su, Y. Liu, Sensors Actuators B: Chem. 382 (2023) 133502.
[34] M. de Celis, L. Serrano-Aguirre, I. Belda, et al., Sci. Total Environ. 799 (2021) 149401.
[35] R. Mukherji, N.K. Varshney, P. Panigrahi, C.G. Suresh, A. Prabhune, Enzyme Microb. Tech. 56 (2014) 1–7.

[36] L.L. Wu, X. Meng, Q. Zhang, et al., Chin. Chem. Lett. 35 (2024) 108663.
[37] Q. Zhang, Q. Wang, S. Xu, et al., Chem. Commun. 53 (2017) 1366–1369.
[38] J. Obszynski, H. Loidon, A. Blanc, J.M. Weibel, P. Pale, Bioorg. Chem. 126 (2022) 105824.
[39] L.L. Wu, Q. Wang, Y. Wang, et al., Chem. Sci. 11 (2020) 3141–3145.
[40] E.C. Eze, H.Y. Chenia, M.E.E. Zowalaty, Infect. Drug Resist. 11 (2018) 2277–2299.
[41] R.A. Arshad, S. Muhammad, Pak. J. Biol. Sci. 3 (2000) 862–865.
[42] K. Rajendran, S. Mahadevan, R. Jeyaprakash, G. Paramasamy, A.B. Mandal, Appl. Biochem. Biotech. 171 (2013) 1328–1338.
[43] S.S. Evstigneeva, D.S. Chumakov, R.S. Tumskiy, B.N. Khlebtsov, N.G. Khlebtsov, Talanta 264 (2023) 124773.
[44] V.N. Nguyen, Z. Zhao, B.Z. Tang, J. Yoon, Chem. Soc. Rev. 51 (2022) 3324–3340.
[45] B. Ran, Z. Wang, W. Cai, et al., J. Am. Chem. Soc. 143 (2021) 17891–17909.
[46] Q. Jia, Q. Song, P. Li, W. Huang, Adv. Healthc. Mater. 8 (2019) e1900608.
[47] K. Yang, F. Long, W. Liu, et al., ACS Appl. Mater. Interfaces 14 (2022) 18043–18052.
[48] D. Yu, Y. Zha, Z. Zhong, et al., Sensors Actuators B: Chem. 339 (2021) 129878.
[49] H. Tang, Y. Liu, B. Li, et al., Bioact. Mater. 6 (2021) 4758–4771.
[50] C. Mao, Y. Xiang, X. Liu, et al., ACS Appl. Mater. Inter. 11 (2019) 17902–17914.